Acta Crystallographica Section D
Biological Crystallography
ISSN 0907-4449

Structure of PduT, a trimeric bacterial microcompartment protein with a 4Fe–4S cluster-binding site

Allan Pang,[a] Martin J. Warren[b] and Richard W. Pickersgill[a]*

[a]School of Biological and Chemical Sciences, Queen Mary University of London, Mile End Road, London E1 4NS, England, and [b]Centre for Molecular Processing, School of Biosciences, University of Kent, Giles Lane, Canterbury, Kent CT2 7NJ, England

Correspondence e-mail: r.w.pickersgill@qmul.ac.uk

Received 19 October 2010
Accepted 1 December 2010

PDB Reference: PduT, 3pac.

Propanediol metabolism in *Citrobacter freundii* occurs within a metabolosome, a subcellular proteinaceous bacterial microcompartment. The propanediol-utilization (Pdu) microcompartment shell is constructed from thousands of hexagonal-shaped protein complexes made from seven different types of protein subunit. Here, the structure of the bacterial microcompartment protein PduT, which has a tandem structural repeat within the subunit and forms trimers with pseudohexagonal symmetry, is reported. This trimeric assembly forms a flat approximately hexagonally shaped disc with a central pore that is suitable for a 4Fe–4S cluster. The essentially cubic shaped 4Fe–4S cluster conforms to the threefold symmetry of the trimer with one free iron, the role of which could be to supply electrons to an associated microcompartment enzyme, PduS.

1. Introduction

Bacterial microcompartments are polyhedral cellular inclusions that consist of a protein shell that encloses a specific metabolic process. The best characterized of these is the carboxysome (Tanaka *et al.*, 2008), which houses the enzymes ribulose bisphosphate carboxylase/oxygenase and carbonic anhydrase. It is thought that the carboxysome accelerates the rate of carbon fixation by increasing the local concentration of carbon dioxide. More recently, similar sequences to the bacterial microcompartment proteins of the carboxysome have been discovered in metabolic operons associated with propanediol utilization (*pdu* genes; Bobik *et al.*, 1999), ethanolamine utilization (Stojiljkovic *et al.*, 1995) and ethanol utilization (Seedorf *et al.*, 2008). In growth conditions that induce these metabolic operons, microcompartments can be seen in the cytoplasm of these bacteria. These metabolic microcompartments are known as metabolosomes (Brinsmade *et al.*, 2005; Parsons *et al.*, 2008).

The 21-gene regulon of *Citrobacter freundii* encoding the *pdu* organelle and propanediol-utilization enzymes (Fig. 1) has been cloned into *Escherichia coli*, resulting in the production of microcompartments and allowing propanediol utilization. Inside the microcompartment, 1,2-propanediol is converted into propionaldehyde by a diol dehydratase composed of PduCDE. Sequestration of propionaldehyde within the microcompartment may prevent unwanted reactions leading to growth arrest and DNA damage (Sampson & Bobik, 2008). The propionaldehyde is subsequently disproportionated into 1-propanol and propionyl-CoA by the aldehyde dehydrogenase PduQ and the CoA transferase PduP, respectively. These two products are delivered out to the cytoplasm, where propionyl-CoA is further converted into propionyl phosphate and propionate by PduL and PduW,

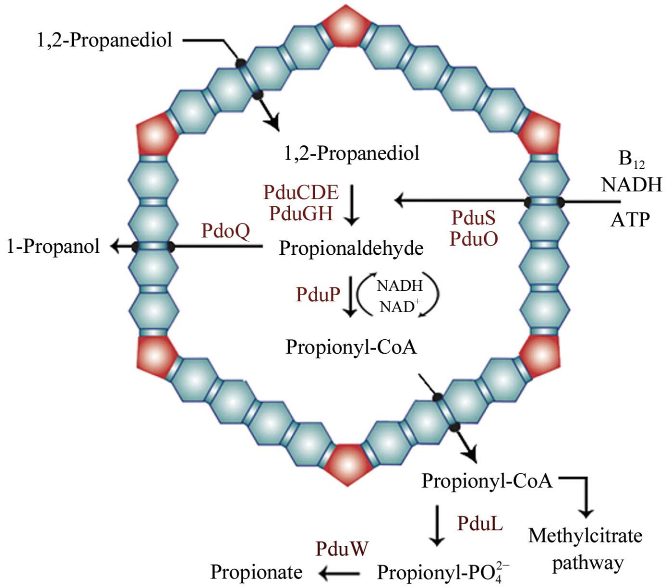

(*a*)

Gene	Function
*pdu*A	Shell protein
*pdu*B	Shell protein
*pdu*C	Diol dehydratase large subunit
*pdu*D	Diol dehydratase medium subunit
*pdu*E	Diol dehydratase small subunit
*pdu*F	Propanediol diffusion facilitator
*pdu*G	Diol dehydratase reactivation protein
*pdu*H	Diol dehydratase reactivation protein
*pdu*J	Shell protein
*pdu*K	Shell protein

Gene	Function
*pdu*L	Phosphotransacylase
*pdu*M	Unknown
*pdu*N	Shell protein
*pdu*O	Cobalamin adenosyltransferase
*pdu*P	CoA-dependent propionaldehyde dehydrogenase
*pdu*Q	Propanol dehydrogenase
*pdu*S	Cobalamin reductase
*pdu*T	Shell protein
*pdu*U	Shell protein
*pdu*V	Unknown
*pdu*W	Propionate kinase
*pdu*X	Unknown

(*b*)

Figure 1
The *C. freundii* propanediol-utilization bacterial microcompartment. (*a*) Schematic representation of the metabolic pathway of the propanediol-utilization bacterial microcompartment. (*b*) A list of the genes involved in the propanediol-utilization metabolosome, including both enzymes and shell proteins (highlighted).

respectively. Not only does the metabolosome contain the enzymes for 1,2-propanediol breakdown, it also contains reactivation factors for the diol dehydratase PduGH as well as enzymes for the formation of the coenzyme form of cobalamin: PduO and PduS. The latter is a corrin reductase and has recently been shown to contain two redox (4Fe–4S) centres (M. J. Warren, unpublished results), the role of which may be to assist in the removal of electrons from the metabolosome.

The Pdu microcompartment capsid, or shell, consists of seven different shell-protein subunits (in order of relative abundance: PduA, PduJ, PduB, PduU, PduK, PduN and PduT; Walter *et al.*, 1997). Sequence comparisons of these shell proteins reveal that the majority of the polypeptide chain

Table 1
Data-collection and refinement statistics.

Values in parentheses are for the highest resolution shell. The values presented in this table were obtained using *SCALA* (Evans, 2006), *REFMAC* (Murshudov *et al.*, 1997) and *PROCHECK* from the *CCP*4 suite (Collaborative Computational Project, Number 4, 1994).

	Native	Osmate soak
Data reduction		
Space group	$P6_3$	$P6_3$
Unit-cell parameters (Å, °)	$a = b = 67.8$, $c = 62.0$, $\alpha = \beta = 90.0$, $\gamma = 120$	$a = b = 67.8$, $c = 61.7$, $\alpha = \beta = 90.0$, $\gamma = 120$
Molecular mass (Da)	18907	18907
Molecules per asymmetric unit	1	1
Osmium sites per asymmetric unit	0	5
Wavelength (Å)	0.933	1.1410
Resolution (Å)	33.84–1.86 (1.96–1.86)	42.53–1.78 (1.82–1.78)
No. of unique reflections	13647 (1979)	15545 (1089)
Multiplicity	8.2 (8.0)	6.6 (5.6–3.0)
Completeness (%)	100 (100)	99.3 (82–95.2)
$R_{\rm merge}$† (%)	0.095 (0.580)	0.045 (0.429)
Mean $I/\sigma(I)$	18.5 (3.7)	21.2 (2.2)
$R_{\rm p.i.m.}$‡ (%)	0.035 (0.22)	0.026 (0.339)
$R_{\rm meas}$§ (%)	0.101 (0.62)	0.07 (0.623)
MSAN¶	—	1.55
Wilson B factor (Å^2)	21.2	26.4
Refinement		
Resolution (Å)	29.71–1.86	
Reflections (work/test)	12258/1372	
R factor/$R_{\rm free}$†† (%)	0.199/0.252	
R.m.s.d. bonds (Å)/angles (°)	1340/1819	
Ramachandran plot statistics, residues in (%)		
Most favoured regions	91.2	
Additional allowed regions	6.9	
Generously allowed regions	1.3	
Disallowed regions	0.6	

† $R_{\rm merge} = \sum_{hkl}\sum_i |I_i(hkl) - \langle I(hkl)\rangle| / \sum_{hkl}\sum_i I_i(hkl)$, where $I_i(hkl)$ is the intensity of the ith observation and $\langle I(hkl)\rangle$ is the mean intensity of the reflection. ‡ $R_{\rm p.i.m.}$ is a measure of the quality of the data taking account of the multiplicity (Weiss, 2001). § $R_{\rm meas}$ (also known as $R_{\rm r.i.m.}$) is an improved version of the traditional $R_{\rm merge}$ (Evans, 2006). ¶ MSAN is the midslope of anomalous normal probability. †† R factor $= \sum_{hkl} ||F_{\rm obs}| - |F_{\rm calc}|| / \sum_{hkl} |F_{\rm obs}|$, where $F_{\rm obs}$ and $F_{\rm calc}$ represent the observed and calculated structure factors, respectively. The R factor is calculated using the 95% of the data that were included in refinement and $R_{\rm free}$ is calculated using the excluded 5%.

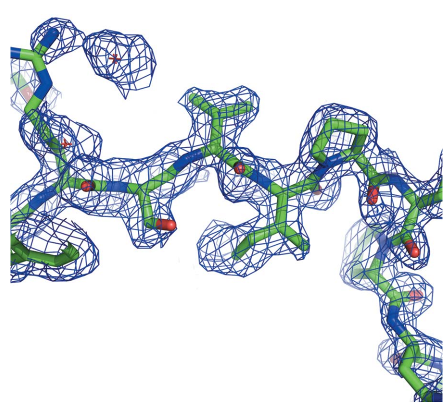

Figure 2
Quality of the electron-density map of PduT. An σ_A-weighted ($2mF_{\rm obs} - DF_{\rm calc}$) Fourier synthesis OMIT map contoured at 1σ showing the quality of the electron density (blue mesh) around Val169 on β8 of PduT is shown. The structure was solved by SAD phasing, exploiting the binding of ammonium hexachloroosmate to the protein. The simple composite OMIT map was calculated using *PHENIX* (Adams *et al.*, 2010). This figure was produced using *PyMOL* (DeLano, 2002).

comprises the bacterial microcompartment (BMC) protein domain (InterPro domain IPR000249). These Pdu shell proteins have a single BMC domain within their sequences and assemble into hexamers, with the exceptions of PduB and PduT. Shell proteins with two BMC domains, for instance EtuB, a closely related protein to PduB, assemble into trimeric (pseudohexameric) structures (Heldt *et al.*, 2009). These shell proteins appear to form the flat facets of the microcompartment capsid (Kerfeld *et al.*, 2005; Tanaka *et al.*, 2008; Yeates *et al.*, 2010), while pentameric units such as those predicted for PduN are thought to form the vertices of the encasement (Yeates *et al.*, 2010; Tanaka *et al.*, 2008). An important characteristic of these shell proteins is the central pore formed by the hexameric (or pseudohexameric) protein assemblies. The central pore is predicted to play a major role in allowing the movement of molecules such as substrates and products into and out of the metabolosome (Kerfeld *et al.*, 2005; Tanaka *et al.*, 2008, 2009; Tsai *et al.*, 2007).

During our initial characterization of the shell proteins, it was discovered that PduT contains a 4Fe–4S cluster. This suggests that the shell proteins not only have pores for substrate and product transit, but may also act as conduits for single electron-transfer processes. PduT has four cysteines; the mutation of one, Cys38, led to the loss of the 4Fe–4S cluster. Although it has been shown that PduT is not essential for bacterial microcompartment formation, it would appear to interact with PduS, the aforementioned corrin reductase, which also contains 4Fe–4S clusters (Parsons *et al.*, 2008). These observations are consistent with the idea that electrons can be passed out of the metabolosome from PduS to PduT. Here, we report the elucidation of the structure of PduT, revealing its trimeric structure and 4Fe–4S binding site.

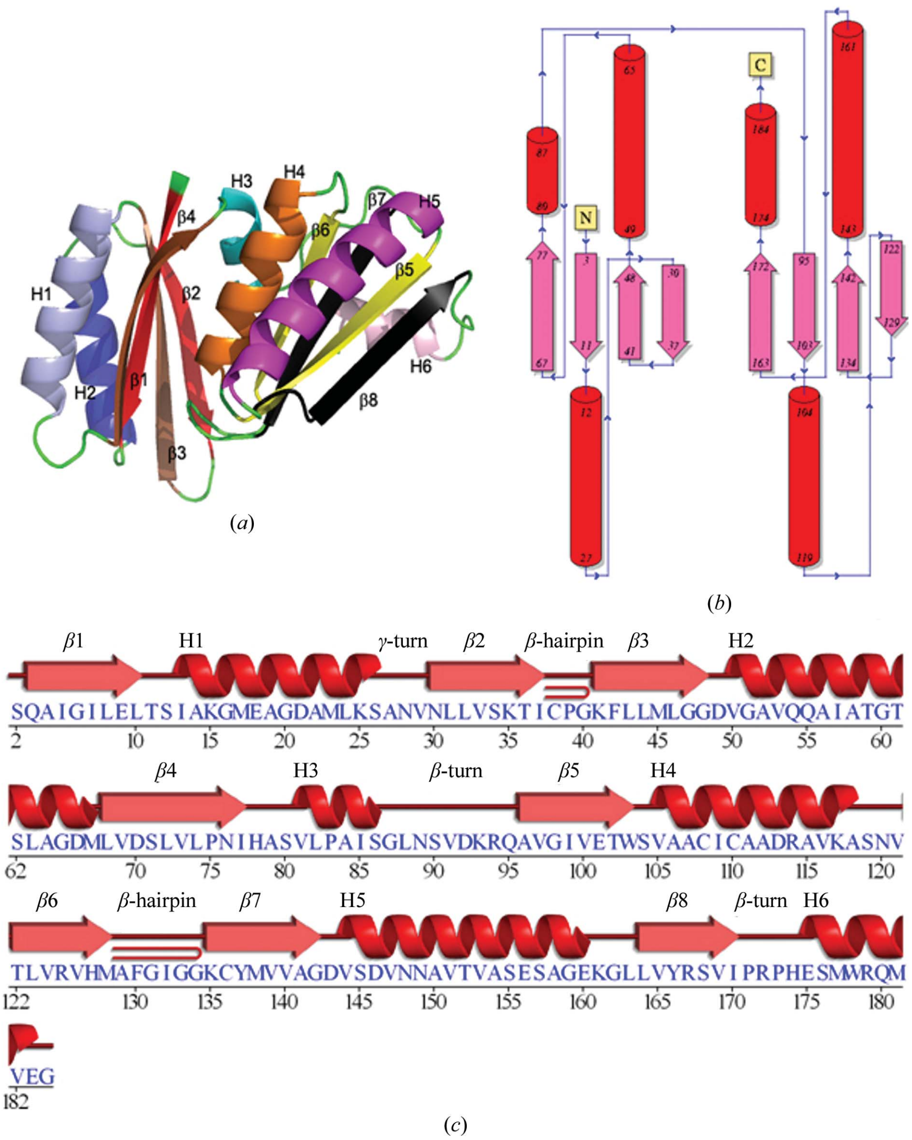

Figure 3
The tertiary structure of the PduT subunit. (*a*) Cartoon representation of the tertiary structure of the PduT subunit, which comprises two BMC repeats. (*b*) Schematic drawing of the topology of the PduT subunit. (*c*) Amino-acid sequence of PduT with secondary structures marked. This figure was produced using *PDBsum* (Laskowski *et al.*, 1997).

2. Materials and methods

2.1. Crystallization of PduT

The coding region of PduT was cloned into pET14b and overproduced and purified as described previously (Parsons *et al.*, 2008). His-tagged PduT was concentrated to 7 mg ml^{-1} in 50 m*M* Tris–HCl pH 7.5. Initial hanging-drop vapour-equilibration crystallization trials using Hampton Research Crystal Screen and Crystal Screen 2 resulted in a small number of conditions yielding small crystals. When the size of the crystals increased to 0.1 mm across they could be seen to be hexagonal plates. The best diffracting crystals were grown using a reservoir consisting of 0.1 *M* bicine buffer pH 8.0, 0.1 *M* NaCl and 25% PEG 550, with hanging drops formed from 2 µl protein solution and 2 µl reservoir mixture. Single crystals were harvested in litholoops, transferred through reservoir supplemented with 15% PEG 400 as a cryoprotectant and stored in liquid nitrogen prior to data collection. To prepare heavy-atom derivatives, 20 PduT crystals were transferred to and soaked in 20 different heavy-atom solutions. One of these soaking conditions, discussed below, was 5 m*M* ammonium hexachloroosmate for 10 min.

2.2. Data collection and structure solution

High-quality diffraction data were collected to 1.86 Å resolution from the native protein on beamline ID14-1 at the European Synchrotron Radiation Facility (Table 1). Some of the crystals were twinned, but this was not a property of all of the screened crystals. Heavy-atom data were collected at the absorption peak as determined from a fluorescence scan of the crystal on beamline I04 at the Diamond Light Source (Oxfordshire, England). The 5 m*M* ammonium hexachloro-osmate-soaked crystal was both untwinned and had a good anomalous signal with peak absorbance at 1.141 Å, the wavelength at which data for single anomalous diffraction phasing were collected (Table 1). Data were reduced using *MOSFLM* (Leslie, 1992) and *SCALA* (Evans, 2006). The hexagonal crystals belonged to space group $P6_3$ and have a single PduT subunit in the asymmetric unit, which gives a solvent content of 43%. The structure was solved using single-wavelength anomalous dispersion phasing, exploiting the anomalous diffraction of the osmate ions, using *PHENIX* (Adams *et al.*, 2010). The resulting structure of PduT was refined against the native data using *REFMAC* (Murshudov *et al.*, 1997) with rebuilding using *Coot* (Emsley *et al.*, 2010). Coordinates and structure-factor amplitudes have been deposited in the PDB with code 3pac.

2.3. Structure analysis

The protein sequence of *C. freundii* PduT was obtained from the NCBI protein database. Sequence alignment of the BMC domains was carried out using *ClustalW* (Larkin *et al.*, 2007; Gouy *et al.*, 2010) and the alignment file was viewed using *SeaView* (Gouy *et al.*, 2010). The trimeric structure of PduT was generated using the *PISA* software (EBI). *PDBsum* was used to make a schematic representation of the topology of the PduT trimer (Laskowski *et al.*, 1997). The structures were visualized and aligned using *PyMOL* (DeLano, 2002).

3. Results and discussion

3.1. Structure solution

PduT was successfully produced and crystallized in space group $P6_3$ and diffraction extended to beyond 1.9 Å resolution. A crystal soaked in 5 m*M* ammonium hexachloroosmate for 10 min before cryocooling diffracted well and gave a good anomalous signal that was suitable for determining experimental protein phases using the single-wavelength anomalous dispersion (SAD) method. The *AutoSol* wizard from *PHENIX* (Adams *et al.*, 2010) found eight osmate sites and gave phases with a figure of merit of 0.340; *AutoBuild* produced a model of 175 residues in six fragments with 85 waters, giving an *R* factor, an $R_{\rm free}$ and a correlation coefficient of 0.223, 0.245 and 0.80, respectively. This model was used in cycles of refinement and rebuilding against the native PduT data to yield the final PduT structure at 1.86 Å resolution (refinement and validation statistics are presented in Table 1). The final model of PduT has a clearly defined polypeptide backbone in the electron-density map for residues 2–184, with the exception of residues 37–41. An example of the electron density is shown in Fig. 2. The residues preceding serine (residue 2) and those in the loop containing residues 37–41 are more flexible and are not clearly defined in the electron-density map. Almost all of the side chains have clearly defined electron density, with the notable exception being Phe130 adjacent to the flexible loop, and some residues exhibit two different conformations. The faint reddish colour of the protein sample suggested the retention of the 4Fe–4S iron–sulfur cluster after elution from the nickel column, but the cluster is not seen in the final structure; this is presumably because the iron–sulfur cluster is oxygen-labile and is lost during crystallization.

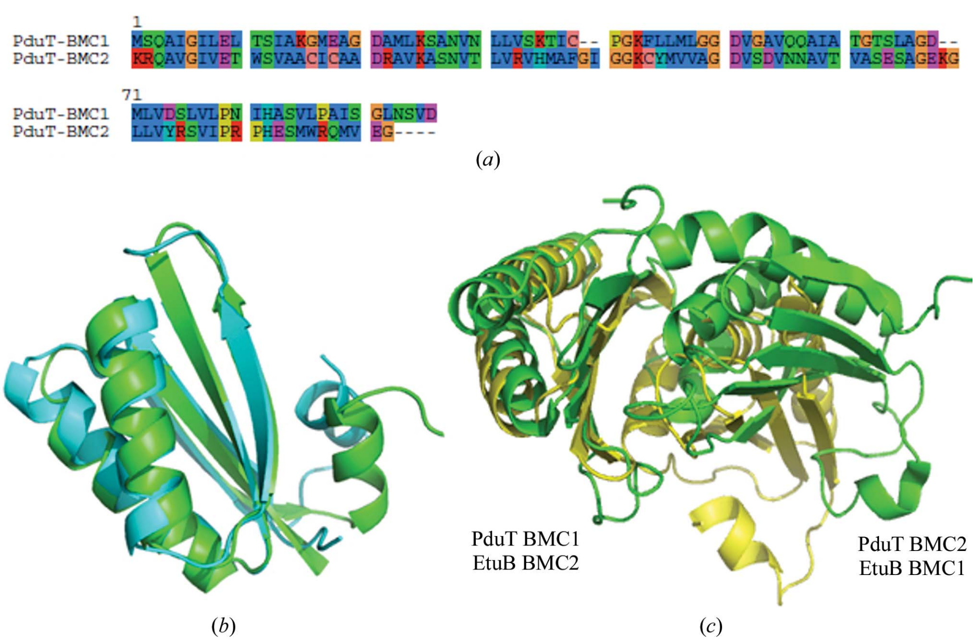

Figure 4
Comparison of the first and second BMC repeats of the PduT subunit. (*a*) The aligned sequences of the first and second BMC repeats and (*b*) superimposition of the BMC domains. (*c*) BMC1 of PduT superimposed on BMC2 of EtuB, showing optimal superimposition of these two proteins. This figure was produced using *PyMOL* (DeLano, 2002).

3.2. Subunit structure

Most shell proteins characterized to date comprise approximately 90 residues and have a single canonical BMC domain. PduT is a 184-residue shell protein with two canonical BMC repeats per subunit. The canonical BMC domains of PduT each consist of two β–α–β motifs connected by a β-hairpin forming an antiparallel β-sheet (Fig. 3). The two BMC domains of the PduT subunit are connected by a short α-helix (H3) and a β-turn. The two BMC domains of PduT have 31.5% sequence identity

(Fig. 4*a*) and superimpose with an r.m.s.d. of 1.25 Å for 396 equivalent atoms; this highlights their structural similarity (Fig. 4*b*). However, the plane of the β-sheet of the second BMC domain is skewed compared with that of the first (Fig. 4*c*), a situation that cannot arise in the single BMC repeat proteins since adjacent subunits are related by a pure rotation.

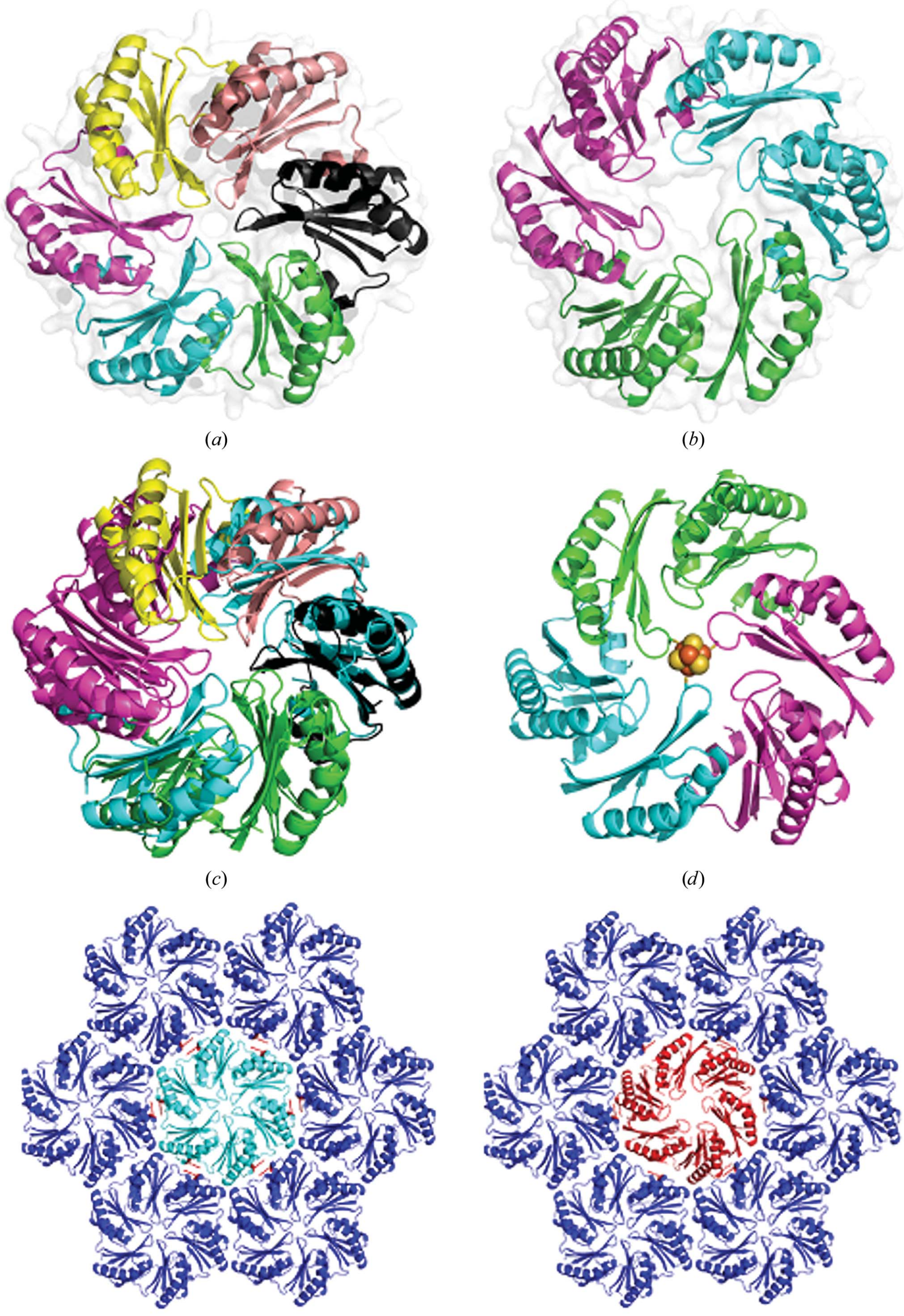

Figure 5
Comparison of quaternary and higher order structures involving PduT. (*a*) The archetypal carboxysome hexamer (CsoS1A hexamer), (*b*) the PduT trimer and (*c*) the CsoS1A hexamer and PduT trimer superimposed. (*d*) A model of the 4Fe–4S iron–sulfur cluster bound to cysteine residues surrounding the central pore of PduT. (*e*) CsoS1A packing in a sheet according to the crystallographic symmetry of the crystal lattice and (*f*) PduT inserted into a sheet of CsoS1A molecules. PduT has approximately the correct dimensions and the lysines (highlighted as red sticks) necessary to form one of the key signature interactions of sheet mosaics. However, PduT does not fit well, suggesting that it would introduce a distortion into a sheet with CsoS1A packing. This figure was produced using *PyMOL* (DeLano, 2002).

3.3. Trimeric structure

Six previously solved shell proteins have a single canonical BMC repeat and form hexamers (Kerfeld *et al.*, 2005; Tsai *et al.*, 2007, 2009; Tanaka *et al.*, 2009, 2010) and two others have a single circularly permuted BMC repeat [EutS (Tanaka *et al.*, 2010) and PduU (Crowley *et al.*, 2008)], while four shell proteins have two BMC domains per subunit with a circularly permutated fold (Tanaka *et al.*, 2010; Klein *et al.*, 2009; Sagermann *et al.*, 2009; Heldt *et al.*, 2009). PduT differs from these as it has a duplication of the canonical BMC domain. The PduT trimer forms a flat approximately hexagonally-shaped disc with a large central pore. The similarity to the archetypal carboxysome shell protein CsoS1A is shown in Figs. 5(*a*)–5(*c*). The central pore is the 4Fe–4S-binding site (Fig. 5*d*). PduT is roughly the correct size to fit into a sheet of carboxysome shell-protein (CsoS1A) molecules (Fig. 5*e*), but is not an exact fit (Fig. 5*f*). The conserved lysines are present, but the spacing between them is too tight for one BMC repeat and too loose for the other. This would introduce a distortion into a flat sheet of molecules and could lead to the generation of curvature, possibly providing an edge to the icosahedral facet.

3.4. Iron–sulfur [4Fe–4S] binding site

The β-hairpin loop from β2 to β3 points towards the pore, producing a threefold arrangement of Cys38 residues about the molecular threefold axis (Fig. 5*d*). This cysteine is implicated in the binding of the 4Fe–4S cluster in PduT, since substitution of this residue caused the characteristic

EPR signal to be lost whereas substitution of two other cysteines did not (Parsons *et al.*, 2008). The 4Fe–4S cluster from *E. coli* ferredoxin (PDB code 2zvs; Saridakis *et al.*, 2009) can be readily fitted into the central pore such that the essentially cubic cluster conforms to the threefold symmetry of the trimer with one sulfur and one iron on the molecular threefold axis (Fig. 4*d*). The cluster can be rotated so that the other three Fe atoms point towards the three Cys38 residues. The conformation of the four-residue β-hairpin is poorly defined in the electron-density map, but it can be readily positioned so as to form S—Fe bonds with the cluster of approximate length 2.3 Å. The on-axis Fe atom could be either up or down and is potentially available to bind another protein; the cluster is accessible from both sides and is therefore in a suitable location for single-electron transfer across the shell of the bacterial microcompartment.

4. Conclusions

The crystal structure of PduT reveals a trimeric arrangement of subunits, each containing a tandem repeat of the canonical BMC domain. The cysteine residue previously shown to bind the 4Fe–4S cluster is positioned such that it could bind three of the four Fe atoms of a 4Fe–4S cluster, leaving the fourth Fe atom free for interaction with another protein such as PduS (Parsons *et al.*, 2008). The structure of PduT strongly suggests that shell proteins modulate not only substrate and product flux but also electron flow. A closely related structure with substituted cysteine has just been published by Yeates and coworkers (Crowley *et al.*, 2010) while we were attempting to obtain crystals with the 4Fe–4S cluster in place. Their work also suggests that PduT binds an iron–sulfur cluster.

This work was supported by the Biotechnology and Biology Research Council (BBSRC), the Higher Education Council of England (HEFCE) and Queen Mary University of London. We acknowledge use of the Diamond Light Source, Oxford and the ESRF, Grenoble.

References

Adams, P. D. *et al.* (2010). *Acta Cryst.* D**66**, 213–221.
Bobik, T. A., Havemann, G. D., Busch, R. J., Williams, D. S. & Aldrich, H. C. (1999). *J. Bacteriol.* **181**, 5967–5975.
Brinsmade, S. R., Paldon, T. & Escalante-Semerena, J. C. (2005). *J. Bacteriol.* **187**, 8039–8046.
Collaborative Computational Project, Number 4 (1994). *Acta Cryst.* D**50**, 760–763.
Crowley, C. S., Cascio, D., Sawaya, M. R., Kopstein, J. S., Bobik, T. A. & Yeates, T. O. (2010). *J. Biol. Chem.* **285**, 37838–37846.
Crowley, C. S., Sawaya, M. R., Bobik, T. A. & Yeates, T. O. (2008). *Structure*, **16**, 1324–1332.
DeLano, W. L. (2002). *PyMOL.* http://www.pymol.org.
Emsley, P., Lohkamp, B., Scott, W. G. & Cowtan, K. (2010). *Acta Cryst.* D**66**, 486–501.
Evans, P. (2006). *Acta Cryst.* D**62**, 72–82.
Gouy, M., Guindon, S. & Gascuel, O. (2010). *Mol. Biol. Evol.* **27**, 221–224.
Heldt, D., Frank, S., Seyedarabi, A., Ladikis, D., Parsons, J. B., Warren, M. J. & Pickersgill, R. W. (2009). *Biochem. J.* **423**, 199–207.
Kerfeld, C. A., Sawaya, M. R., Tanaka, S., Nguyen, C. V., Phillips, M., Beeby, M. & Yeates, T. O. (2005). *Science*, **309**, 936–938.
Klein, M. G., Zwart, P., Bagby, S. C., Cai, F., Chisholm, S. W., Heinhorst, S., Cannon, G. C. & Kerfeld, C. A. (2009). *J. Mol. Biol.* **392**, 319–333.
Larkin, M. A., Blackshields, G., Brown, N. P., Chenna, R., McGettigan, P. A., McWilliam, H., Valentin, F., Wallace, I. M., Wilm, A., Lopez, R., Thompson, J. D., Gibson, T. J. & Higgins, D. G. (2007). *Bioinformatics*, **23**, 2947–2948.
Laskowski, R. A., Hutchinson, E. G., Michie, A. D., Wallace, A. C., Jones, M. L. & Thornton, J. M. (1997). *Trends Biochem. Sci.* **22**, 488–490.
Leslie, A. G. W. (1992). *Jnt CCP4/ESF–EACBM Newsl. Protein Crystallogr.* **26**.
Murshudov, G. N., Vagin, A. A. & Dodson, E. J. (1997). *Acta Cryst.* D**53**, 240–255.
Parsons, J. B. *et al.* (2008). *J. Biol. Chem.* **283**, 14366–14375.
Sagermann, M., Ohtaki, A. & Nikolakakis, K. (2009). *Proc. Natl Acad. Sci. USA*, **106**, 8883–8887.
Sampson, E. M. & Bobik, T. A. (2008). *J. Bacteriol.* **190**, 2966–2971.
Saridakis, E., Giastas, P., Efthymiou, G., Thoma, V., Moulis, J. M., Kyritsis, P. & Mavridis, I. M. (2009). *J. Biol. Inorg. Chem.* **14**, 783–799.
Seedorf, H., Fricke, W. F., Veith, B., Brüggemann, H., Liesegang, H., Strittimatter, A., Miethke, M., Buckel, W., Hinderberger, J., Li, F., Hagemeier, C., Thauer, R. K. & Gottschalk, G. (2008). *Proc. Natl Acad. Sci. USA*, **105**, 2128–2133.
Stojiljkovic, I., Bäumler, A. J. & Heffron, F. (1995). *J. Bacteriol.* **177**, 1357–1366.
Tanaka, S., Kerfeld, C. A., Sawaya, M. R., Cai, F., Heinhorst, S., Cannon, G. C. & Yeates, T. O. (2008). *Science*, **319**, 1083–1086.
Tanaka, S., Sawaya, M. R., Phillips, M. & Yeates, T. O. (2009). *Protein Sci.* **18**, 108–120.
Tanaka, S., Sawaya, M. R. & Yeates, T. O. (2010). *Science*, **327**, 81–84.
Tsai, Y., Sawaya, M. R., Cannon, G. C., Cai, F., Williams, E. B., Heinhorst, S., Kerfeld, C. A. & Yeates, T. O. (2007). *PLoS Biol.* **5**, e144.
Tsai, Y., Sawaya, M. R. & Yeates, T. O. (2009). *Acta Cryst.* D**65**, 980–988.
Walter, D., Ailion, M. & Roth, J. (1997). *J. Bacteriol.* **179**, 1013–1022.
Weiss, M. S. (2001). *J. Appl. Cryst.* **34**, 130–135.
Yeates, T. O., Crowley, C. S. & Tanaka, S. (2010). *Annu. Rev. Biophys.* **39**, 185–205.